

A Novel Method for Determining the Nature of Time Series

Temujin Gautama, Danilo P. Mandic*, *Member, IEEE*, and Marc M. Van Hulle, *Senior Member, IEEE*

Abstract—The delay vector variance (DVV) method, which analyzes the nature of a time series with respect to the prevalence of deterministic or stochastic components, is introduced. Due to the standardization within the DVV method, it is possible both to statistically test for the presence of nonlinearities in a time series, and to visually inspect the results in a DVV scatter diagram. This approach is convenient for interpretation as it conveys information about the linear or nonlinear nature, as well as about the prevalence of deterministic or stochastic components in the time series, thus unifying the existing approaches which deal either with only deterministic versus stochastic, or the linear versus nonlinear aspect. The results on biomedical time series, namely heart rate variability (HRV) and functional Magnetic Resonance Imaging (fMRI) time series, illustrate the applicability of the proposed DVV-method.

Index Terms—fMRI, HRV, nonlinearity analysis, surrogate data.

I. INTRODUCTION

ANALYZING the nature of biomedical time series has received considerable attention in recent years, as the presence of nonlinearity and/or determinism in a physiological signal can often be used as an indicator of the health status of a patient (see, e.g., [1]–[4]). In general, performing a nonlinearity analysis in a modeling or signal processing context can lead to a significant improvement of the quality of the results, since it facilitates the selection of appropriate processing methods, suggested by the data itself, e.g., using linear or nonlinear filters. Indeed, since the training of nonlinear models and filters is more complex and less convenient than that of their linear counterparts, these models should be avoided when the signals

are actually linear in nature. A comprehensive account of the importance of this class of analysis in engineering, medicine and earth sciences, and an introduction to basic methods is given in [5].

The existing methods for the analysis of the nonlinear nature of a time series are twofold: in one case, different models (e.g., linear and nonlinear ones) are fit to the time series and their accuracies are evaluated [1], [4], [6], whereas in the other case, certain nonlinearity measures computed for the signal under study are compared to those obtained for linearized versions of the data, so-called surrogates (for an overview, see [7]). Another aspect of a time series, which is based on the Wold decomposition theorem [8], highlights the prevalence of the deterministic or stochastic component of a time series, a property which can also be examined using the method introduced in [6].

The presence of (non-) linear deterministic or stochastic behavior in a biomedical signal conveys important information. A change in the nature of a monitored signal might indicate a change in the health condition. This paper, therefore, considers the problem of determining the nature of a biomedical signal: how we can judge about the nature of a time series, given that it is recorded under an unknown measurement condition and possibly through a nonlinear observation function. The work presented here differs from much previous work in that it takes into consideration both the linear or nonlinear, and the deterministic or stochastic aspects of a time series. We propose a unifying method for sequentially analyzing the deterministic or stochastic nature [delay vector variance (DVV) method], and the linear or nonlinear nature (DVV scatter diagram). The first analysis characterizes a time series in a standardized manner, whereas the latter additionally employs the concept of surrogate data. The proposed DVV method is applied to two types of biomedical signals, namely to HRV and fMRI time series, and the results are in line with those obtained using other methods from the literature. They confirm current hypotheses on the presence of nonlinearities in biomedical time series, while the proposed method further provides an account of another aspect of the time series, namely the deterministic or stochastic nature.

II. TIME SERIES USED

A. Benchmark Time Series

The proposed method is first verified on four benchmark time series of 1000 samples, three of which are synthetically generated and the remaining one is a real-world time series. The first synthetic time series is a realization of the Hénon Map, given by

$$x_k = 1 - a x_{k-1}^2 + b y_{k-1}$$

$$y_k = x_{k-1}$$

Manuscript received January 29, 2002; revised August 15, 2003. The of T. Gautama was supported by the Flemish Regional Ministry of Education under Scholarship GOA 2000/11 and in part by the Fund for Scientific Research under Grant G.0248.03. The work of D. P. Mandic was supported by the European Commission, 5th framework programme under Grant QLG3-CT-2000-30161 and in part by the K.U.Leuven unde visiting fellowship F/01/079) while at the Laboratorium voor Neuro- & Psychofysiologie, K.U.Leuven, Belgium. The work of M. M. Van Hulle was supported in part by the Fund for Scientific Research under Grant G.0185.96N and G.0248.03, in part by the National Lottery (Belgium) under Grant 9.0185.96, in part by the Flemish Regional Ministry of Education (Belgium) under Grant GOA 95/99-06 and Grant 2000/11, in part by the Flemish Ministry for Science and Technology under Grant VIS/98/012), and in part by the European Commission, 5th framework programme under Grant QLG3-CT-2000-30161 and Grant IST-2001-32114. The authors are solely responsible for the contents of this paper. It does not represent the opinion of the Community, and the Community is not responsible for any use that might be made of data appearing therein. *Asterisk indicates corresponding author.*

T. Gautama and M. M. Van Hulle are with the Laboratorium voor Neuro- en Psychofysiologie, K.U.Leuven, Leuven, Belgium.

*D. P. Mandic is with the Department of Electrical and Electronic Engineering, Imperial College of Science, Technology and Medicine, London, SW7 2BT U.K.

Digital Object Identifier 10.1109/TBME.2004.824122

where $a = 1.4$ and $b = 0.3$. Next, a realization of the Mackey-Glass equation is considered, namely

$$\frac{dx}{dk} = \frac{0.2x_{k-\tau}}{1 + x_{k-\tau}^{10}} - 0.1x_k$$

where $\tau = 17$, which is solved numerically using the fourth-order Runge-Kutta method with an integration step of 0.01 and a sampling rate of 6. Unlike the previous two nonlinear benchmark signals, the third consists of colored noise generated from a stable AR(4)-model (a linear stochastic model)

$$x_k = 1.79x_{k-1} - 1.85x_{k-2} + 1.27x_{k-3} - 0.41x_{k-4} + \nu_k$$

where ν_k is a white noise source with a standard normal distribution. Finally, the real-world benchmark time series consists of intensity measures from a Far-Infrared-Laser in a chaotic state, which has been used in the Santa Fe competition [9].

B. Biomedical Time Series

Six Heart Rate Variability (HRV) time series have been derived from long-term electrocardiogram recordings (14–22 h each), with manually reviewed beat annotations, taken from the MIT-BIH Long-Term database.¹ The time series are labeled A1–A6 for, respectively, record numbers 14046, 14149, 14157, 14172, 14184, and 15814. The signals consist of recordings of male patients suffering from different heart diseases. For efficiency, the time series have been limited in size to 8192 samples. It is generally accepted that the heart condition influences the nonlinear nature of the HRV signal [1]–[4].

The functional Magnetic Resonance Imaging (fMRI) time series have been taken from two experimental macaque motion studies [10]. We consider four time series, taken from the left and right middle temporal area (MT/V5), recorded using two different contrast agents: one set (time series labeled B1 and B2, 1920 samples) is recorded using the traditional blood oxygen level dependent (BOLD) contrast agent, and the other (time series B3 and B4, 1200 samples) using an exogenous contrast agent, namely monocrySTALLINE iron oxide nanoparticle (MION), which has been recently introduced for application in fMRI. The latter is expected to be dependent on fewer physiological variables which possibly interact in a nonlinear fashion, and should, therefore, display less nonlinearity than the BOLD signals [11].

III. THE DELAY VECTOR VARIANCE METHOD

We propose a novel, unifying time series analysis methodology, which separately examines two aspects, namely the degree to which it is deterministic or stochastic, and whether it is linear or nonlinear. In this context, it is convenient to use the method of time-delay embedding, i.e., to represent a time series as a set of delay vectors (DVs) of a given embedding dimension m , denoted by $\mathbf{x}(k) = [x_{k-m\tau}, \dots, x_{k-\tau}]$, where the subscript indexes time and τ is a time lag which is set to unity throughout the simulations. Every DV $\mathbf{x}(k)$ is associated with a corresponding *target*, namely the next sample, x_k .

¹Publicly available from <http://www.physionet.org/physiobank/database/ltldb/>.

We next start with the description of the technique of surrogate data and proceed with the analysis of deterministic versus stochastic and linear versus nonlinear nature of a signal.

Surrogate Data

A surrogate time series is a realization of a null hypothesis, which in our case is that the original time series is linear. There exist many methods for generating surrogates (for an overview, see [7]). We have opted for the approach introduced in [12], the iterative amplitude adjusted Fourier transform (iAAFT) approach, since it has been observed to yield superior results compared to other methods (see, e.g., [7] and [13]). This type of surrogate time series retains the signal distribution and amplitude spectrum² of the original time series, and takes into account a possibly nonlinear and static observation function due to the measurement process. The method uses a fixed point iteration algorithm for achieving this, for the details of which we refer to [7] and [12]. For the simulations in this paper, 99 surrogates have been generated for each of the time series under study.

A. Deterministic or Stochastic?

The Wold decomposition theorem [8] states that any discrete, stationary signal can be decomposed into a *deterministic*³ and a *stochastic* (random) component, which are uncorrelated. Therefore, rather than making a decision between deterministic and stochastic, the predictability of a time series, which is closely related to the prevalence of the deterministic component, is examined in this stage of the analysis. Furthermore, it will allow for a standardized characterization of a time series which can be used for nonlinearity testing in the next stage.

The proposed DVV analysis is based upon the “target variance,” σ^{*2} , which is an inverse measure of the predictability of a time series for a given embedding dimension, m . A set $\Omega_k(m, r_d)$ is generated by grouping those DVs that are within a certain Euclidean distance, r_d , to $\mathbf{x}(k)$, which is varied in a manner standardized with respect to the distribution of pairwise distances between DVs. For a given embedding dimension m , the proposed “*delay vector variance*” method can be summarized as follows.

- The mean, μ_d , and standard deviation, σ_d , are computed over all pairwise distances between DVs.
- The spans, r_d , are taken from the interval $[\mu_d - n_d\sigma_d; \mu_d + n_d\sigma_d]$, e.g., uniformly spaced, where n_d is a parameter controlling the span over which to compute the DVV-plot. The set $\Omega_k(m, r_d)$ consists of all DVs that lie within a distance to $\mathbf{x}(k)$ equal to the span r_d .
- For every set $\Omega_k(m, r_d)$, the variance of the corresponding targets is computed. The average over all sets, divided by the variance of the time series, yields the inverse measure of predictability, namely the ‘target variance’, $\sigma^{*2}(m, r_d)$. We only compute the variance if $\Omega_k(m, r_d)$ contains at least $N_o = 30$ DVs.

As a result of the standardization of the distance axis, the resulting “DVV-plot,” i.e., the target variance $\sigma^{*2}(m, r_d)$ as a

²The amplitude spectrum can be used as an estimate of the autocorrelation spectrum due to the Wiener-Khinchin theorem.

³A deterministic signal is one for which the generation process can be described precisely by a set of linear or nonlinear equations.

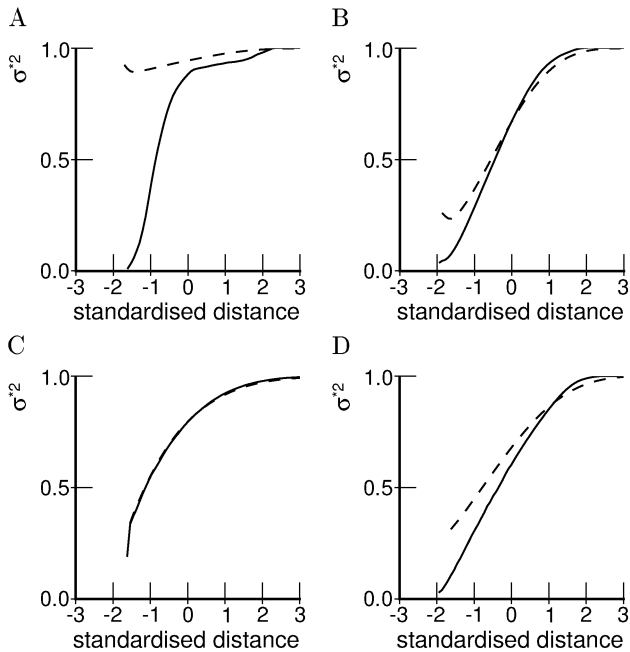


Fig. 1. Solid curves represent the DVV-plots for the Hénon Map (A), Mackey-Glass (B), colored noise (C), and the laser time series (D). Average DVV-plots computed over 99 surrogates are shown as dashed curves.

function of the span r_d for a given embedding dimension m , is easy to interpret. This is illustrated in Fig. 1 for the four benchmark signals (solid curves). Note that the units on the horizontal axis denote *standardized* distances, rather than distances as such, since this allows for easier comparison between DVV-plots. The presence of a deterministic component will lead to small target variances for small spans (on the left-hand side of the DVV-plots), and the minimal target variance in a DVV-plot (for a given embedding dimension), $\sigma_{\min}^{*2}(m)$, is related to the prevalence of the deterministic component over the stochastic one. Indeed, a small target variance indicates that similar DVs have similar targets. Therefore, given m previous samples, the time series is well predictable, indicating the presence of a strong deterministic component. The DVV-plots obtained for the Hénon Map, the Mackey-Glass and laser time series [Fig. 1(A), (B) and (D), solid curves] clearly show such a strong deterministic component, whereas this component is weaker for the linearized (and randomized) versions (dashed curves), the so-called surrogates (see below). The colored noise [Fig. 1(C)] also has a deterministic component, albeit a weaker one, and the predictability is the same for the original time series (solid curve) and the linearized version (dashed curve). Furthermore, a DVV-plot smoothly converges to unity at the extreme right, since for maximal spans, *all* DVs belong to the same set, and the variance of the targets is equal to the variance of the time series. If this is not the case, the span parameter n_d should be increased. In all simulations performed in this paper, $n_d = 3$ was sufficient.

The “optimal” embedding dimension can be determined by running a number of DVV-analyses for different values of m , and choosing that for which the minimal target variance (over all spans r_d), $\sigma_{\min}^{*2}(m)$ is minimal. The reasoning behind this approach is that, using this embedding dimension, the best

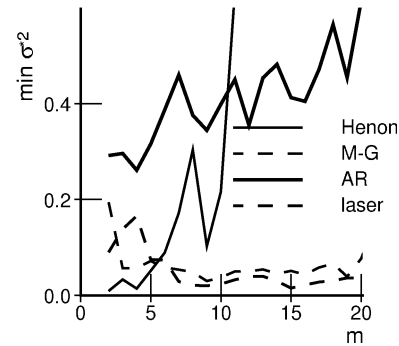


Fig. 2. Minimal target variance σ^{*2} as a function of embedding dimension m for the benchmark time series (conventions as shown in legend).

predictability is obtained, and, correspondingly, this yields the lowest minimal target variance. A similar approach has been adopted in [14]. Examples are shown for the benchmark signals in Fig. 2, yielding optimal embedding dimensions of 2, 9, 4, and 15, respectively for the Hénon Map, Mackey-Glass, colored noise and laser time series. These values have been used for generating the DVV-plots in Fig. 1 and are used in the following nonlinearity analysis.

The minimal target variance, σ_{\min}^{*2} , yields an inverse measure for the predictability of the time series under study, which is closely related to the prevalence of the deterministic component over the stochastic one. It is important to note, however, that it can only be used as a relative, and not as an absolute measure of the prevalence of the deterministic component, since it is dependent on the number of time samples, N , of the time series under study, and the minimal subset size, N_o , in the DVV analysis. To illustrate this sensitivity, the Hénon Map and the colored noise series were considered with an increasing number of time samples, N , for each of which 100 different realizations were generated. These have been analyzed using the DVV method, and the mean minimal target variances (along with the standard deviations) are shown in Fig. 3(A) (the results for the Hénon Map as a solid curve and those for the colored noise series as a dashed curve). There is a clear effect on the minimal target variance for relatively short time series, which becomes less pronounced for $N \geq 1000$. Similarly, to examine the effect of the minimal subset size, N_o , required for computing the variance of the targets in a subset, 100 realizations of $N = 1000$ samples of the Hénon Map and the colored noise series were analyzed using different values for N_o . There is also a clear effect of perturbations on this parameter, as can be seen in Fig. 3(B). The results for the colored noise series (dashed curve) show a monotonic increase of the minimal target variance, σ_{\min}^{*2} , as a function of the minimal set size, N_o , which is to be expected, since larger set sizes correspond to larger regions in phase space, and, accordingly to a larger target variance. The results for the Hénon Map, however, do not show a monotonic increase of the target variance, which is due to the clear phase portrait of the time series [Fig. 3(C)], which is absent in the colored noise series. Indeed, the variances of the targets of subsets in the region labeled “1” in Fig. 3(C), will increase monotonically as the subset size increases, but this is not the case for subsets in the region labeled “2”: for very small regions, the subsets will contain DVs from a single trajectory in phase space, yielding a small variance of

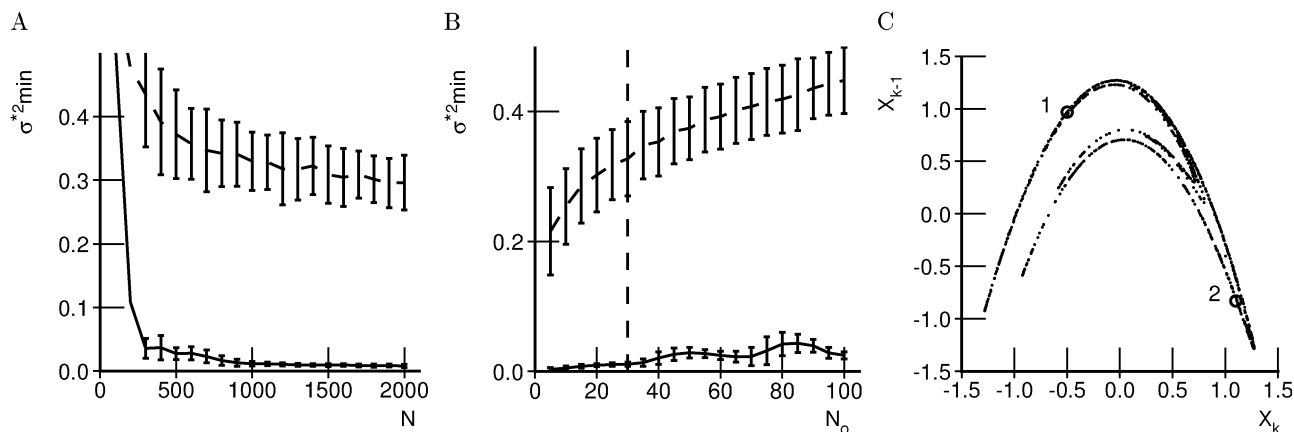


Fig. 3. (A) Parameter sensitivity of the minimal target variance, σ_{\min}^{*2} with respect to the length of the time series, N and (B) with respect to the minimal set size, N_o , for the Hénon Map (solid curve) and the colored noise series (dashed curve). Error bars denote standard deviations and the dashed line in Fig. B shows the default value used in the simulations. (C) Phase space representation of the Hénon Map for an embedding dimension of $m = 2$.

the targets, but when the subset size increases, the neighboring trajectory will be included, due to which the corresponding variance of the targets will increase significantly. Moreover, since the target variance is computed as the mean over the different (valid) subsets, the effect of the minimal subset size, N_o , on the minimal target variance can be very irregular, as can be observed in Fig. 3(B). Therefore, the minimal target variance should only be used for as a comparative measure between time series of the same lengths, using a fixed value for N_o . The dashed line at $N_o = 30$ in Fig. 3(B) represents the default value used in all simulations.

B. Linear or Nonlinear?

For the analysis of the nonlinear nature of a time series, the methodology suggested in [15] is adopted. A “surrogate time series” is generated as a realization of a certain null hypothesis (in our case: linearity) and the DVV-plots are generated for both the surrogate and the original time series. If the DVV-plots are significantly different, the null hypothesis is rejected, and the original time series is considered nonlinear in nature. To visualize and qualify the results, we propose the “DVV scatter diagrams,” in which the target variances averaged over a number of surrogate time series (dashed curves in Fig. 1) are plotted against those of the original time series (solid curves in Fig. 1) for corresponding standardized distances. Examples are shown in Fig. 4 for the benchmark time series. Note that this is possible due to the standardization of the distance axes in the DVV-plots of the original and surrogate time series: a point in the scatter diagram is obtained for identical *standardized* distances. Furthermore, the target variances for a standardized distance are only plotted if there are valid target variances for both the original time series and all of the surrogates, due to which the minimal target variance in the original DVV-plot can be different from that observed in the DVV scatter diagrams [compare, e.g., Fig. 1(A) to Fig. 4(A)]. If the DVV scatter diagram coincides with the bisector line, the time series is linear. Conversely, if the original time series is nonlinear, the curve deviates from the bisector line. Thus, the deviation from the bisector line is an indication of a deviation from the null hypothesis of linearity, and can be quantified by the root-mean-square error (RMSE)

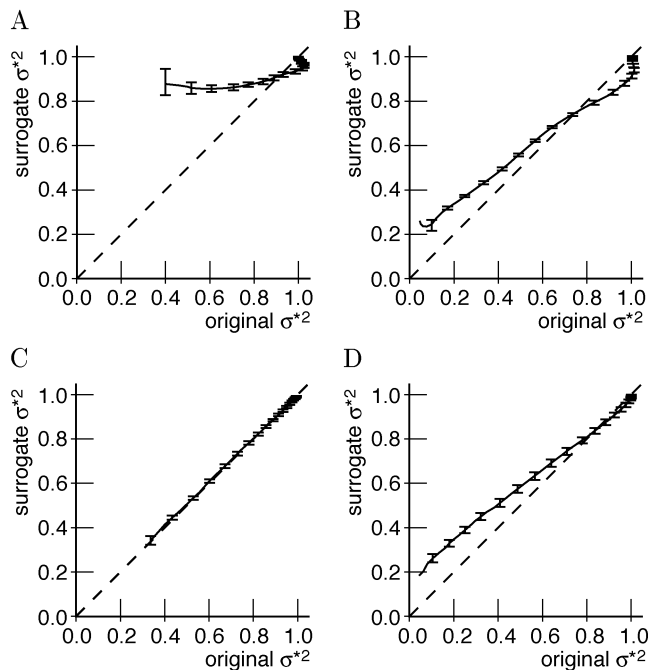


Fig. 4. DVV scatter diagrams for the benchmark time series: Hénon Map (A), Mackey-Glass (B), colored noise, (C) and laser time series (D). The error bars correspond to the upper and lower quartiles of the target variances for the surrogates.

between the σ^2 s of the original time series and the σ^2 s averaged over the DVV-plots of the surrogate time series (note that while computing this average, as well as with computing the RMSE, only the valid measurements are taken into account). In this way, a single test statistic is obtained, which is further used for testing the validity of the null hypothesis. Since the analytical form of the probability distributions of the RMSE is not known, a nonparametric rank-based test is used, as suggested in [16]. For every original time series, we generate 99 surrogates and compute the test statistics for both the original and surrogate time series. These values are sorted in increasing order, and a right-tailed (left-tailed) test is rejected at the level of $\alpha = 0.10$ if rank r of the original time series exceeds 90 (is smaller or equal to 10), and a two-tailed test is rejected if rank r is greater

than 95, or smaller or equal to 5. For the proposed approach, a high RMSE indicates nonlinearity, implying right-tailed testing.

IV. SIMULATIONS

The results obtained using the proposed DVV method are compared to those obtained using other well-established nonlinearity detection methods. The first method we consider is a model-based one, described in [1]. It compares the prediction performances of a linear AR-model and a nonlinear model (second-order Volterra), for both of which the optimal orders (embedding dimension and number of cross-terms in the Volterra series) are chosen using Akaike's information criterion [17]. The prediction gain is defined as

$$\gamma[dB] = 10 \log_{10} \left(\frac{\sigma_{\text{lin}}^2}{\sigma_{\text{nl}}^2} \right)$$

where σ_{lin}^2 and σ_{nl}^2 are the in-sample variances of the linear and nonlinear residuals. For a positive gain, one can conclude that the time series is nonlinear, whereas a null gain indicates that either the time series is linear, or that its nonlinear nature cannot be modeled using a second-order Volterra.

The other two nonlinearity detection methods are the third-order autocovariance (C3) and the asymmetry due to time reversal (REV), both of which have been used in the framework of surrogate data testing in [18]. The first (C3) is a higher-order extension of the traditional autocovariance and is given by

$$C3(\tau) = \langle x_k x_{k-\tau} x_{k-2\tau} \rangle$$

where τ is a time lag. The REV method measures the asymmetry due to time reversal, which has been shown to be useful for detecting nonlinearity in a time series [19]. It can be measured using the following metric [18]

$$REV(\tau) = \langle (x_k - x_{k-\tau})^3 \rangle$$

where again, τ is a time lag. As is the case for the DVV method, the test statistics are computed for the original and 99 surrogate time series, after the nonparametric rank-based (two-tailed) testing is applied. In the analyses of the benchmark time series, the time lags are chosen by considering a range of values and manually selecting the smallest time lag for which the signal is correctly judged to be (non-) linear (at a significance level of $\alpha = 0.10$). Note that this procedure cannot be used in practice, since prior knowledge regarding the linear or nonlinear nature of the signal under study is required. Furthermore, it favors the results obtained by C3 and REV, as the parameters for these tests are optimized and specifically tuned to yield the correct results. For the biomedical time series under study, the time lag was determined as that for which the time-delayed mutual information (TDMI) exhibits a clear minimum [20], [21]. The latter can be approximated by [21]

$$A(\tau) = - \sum_{ij} p_{ij}(\tau) \ln \frac{p_{ij}(\tau)}{p_i p_j}$$

TABLE I

RESULTS FROM THE NONLINEARITY TESTS: PREDICTION GAIN (γ), RANKS OBTAINED USING THE THIRD-ORDER AUTOCOVARIANCE (C3), THE ASYMMETRY DUE TO TIME REVERSAL (REV) AND THE PROPOSED METHOD (DVV AND THE CORRESPONDING RMSE). THE OPTIMAL EMBEDDING DIMENSIONS OBTAINED USING THE MINIMAL TARGET VARIANCES ARE SHOWN IN THE COLUMN LABELED " m_{opt} ," AND THE TIME LAGS USED FOR THE C3 AND REV ANALYSES IN THE COLUMNS LABELED " τ_{C3} " AND " τ_{REV} ," RESPECTIVELY. SIGNIFICANT DETECTIONS OF SIGNAL NONLINEARITY (AT THE LEVEL OF $\alpha = 0.10$) FOR C3, REV AND DVV ARE INDICATED BY BOXES. IN THE FIRST COLUMN, MACKEY-GLASS AND THE COLORED NOISE ARE LABELED AS "M-G" AND "AR," AND THE OTHER TIME SERIES ARE LABELED AS DESCRIBED IN SECTION IV-A

	γ [dB]	C3	τ_{C3}	REV	τ_{REV}	m_{opt}	DVV	RMSE
Hénon	0.54	100	1	1	1	2	100	$9.86 \cdot 10^{-2}$
M-G	6.36	5	2	1	2	9	100	$5.13 \cdot 10^{-3}$
AR	0.02	48	1	76	1	4	25	$3.20 \cdot 10^{-5}$
laser	1.98	1	1	1	7	15	100	$7.74 \cdot 10^{-3}$
A1	0.03	100	10	1	10	19	100	$3.16 \cdot 10^{-2}$
A2	0.02	100	2	71	2	7	100	$9.11 \cdot 10^{-4}$
A3	0.16	100	4	2	4	8	100	$5.99 \cdot 10^{-2}$
A4	0.36	24	5	100	5	22	100	$6.90 \cdot 10^{-2}$
A5	0.02	49	4	1	4	12	100	$4.36 \cdot 10^{-2}$
A6	0.15	100	4	2	4	19	100	$7.28 \cdot 10^{-3}$
B1	0.07	32	3	97	3	21	100	$6.48 \cdot 10^{-3}$
B2	-0.02	62	3	48	3	16	100	$4.84 \cdot 10^{-3}$
B3	-0.08	100	3	98	3	15	83	$4.57 \cdot 10^{-4}$
B4	0.00	100	3	24	3	11	100	$7.57 \cdot 10^{-4}$

where p_i is the probability to find a signal value in the i th interval, and $p_{ij}(\tau)$ is the joint probability of finding a signal value in the i th interval, and a value at time τ later in the j th interval. The probabilities are estimated using a binning approach (200 bins).

A. Benchmark Time Series

The optimal embedding dimensions are obtained by determining the value of m for which the minimal target variance is lowest, as shown in Fig. 2, yielding 2, 9, 4, and 15, respectively for the Hénon Map, Mackey-Glass, colored noise and laser time series. The DVV-plots computed for the optimal embedding dimensions are shown in Fig. 1(A)–(D) for the original (solid curves) time series, together with the DVV-plots averaged over all surrogates (dashed curves). Clearly, the colored noise is more stochastic in nature than the other three time series, since its minimal target variance (the minimum value in the DVV-plot) is fairly large ($\sigma_{\text{min}}^2 = 0.26$). Furthermore, the amount of determinism in the colored noise can be attributed to the linear correlations present in the time series, since the DVV-plots for the surrogates show the same degree of predictability [Fig. 1(C), dashed curve].

The quantitative results from the nonlinearity tests are summarized in Table I. The time lags for C3 and REV, which have been determined by optimizing the detection performance, as described earlier, are shown in columns four and six. All

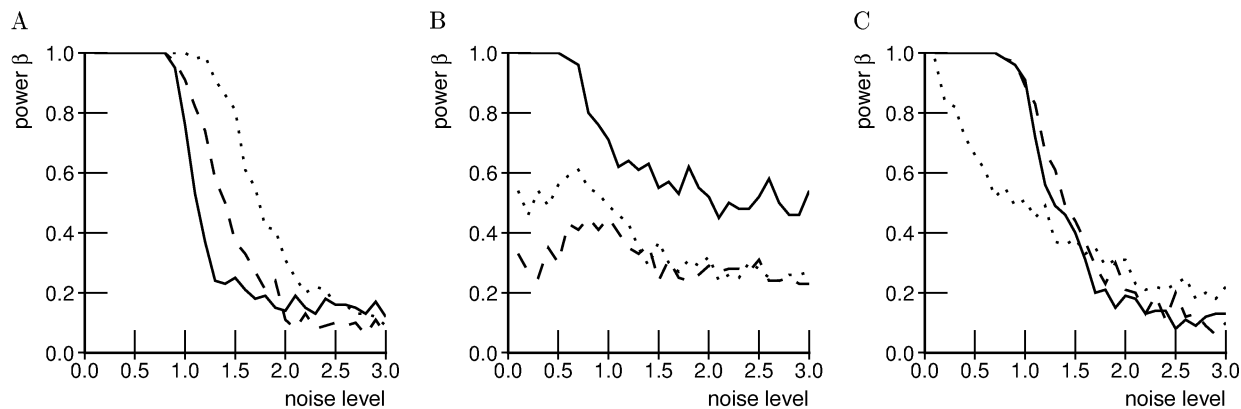


Fig. 5. Estimated power for C3 (dashed), REV (dotted) and DVV (solid) as a function of the noise level for (A) the Hénon Map, (B) Mackey-Glass, and (C) laser time series.

methods correctly judge the natures of the nonlinear, as well as the linear time series. The corresponding DVV scatter diagrams are shown in Fig. 4 (the error bars denote the upper and lower quartiles, of which only one in three is shown). Qualitatively, it is clear that the deviation from the bisector line, and thus, from the null hypothesis of linearity, is strongest for the Hénon Map, which can also be concluded from the RMSE value in Table I, contrary to the results for the prediction gain, where the Mackey-Glass time series yields the highest gain.

We have further performed a noise analysis to examine the robustness of the various methods. As suggested in [18], the power of the test, β , is estimated for different levels of in-band noise by determining the ratio of correct rejections of the null hypothesis of linearity. The nonlinearity tests were performed at a significance level of $\alpha = 0.10$ using $N_s = 19$ surrogates. The in-band noise, ν_k , consists of phase-randomized versions of the time series under study, and is added to the time series using:

$$x_k = \sqrt{\frac{1}{1+a^2}}(x_k + a\nu_k)$$

where a is a factor controlling the noise level. The results are shown in Fig. 5(A)–(C), respectively for the Hénon Map, Mackey-Glass and laser time series. The parameter values shown in Table I have been used throughout these analyses. The power, β , is more robust to noise for C3 and REV than for the DVV method in the case of the Hénon Map. In a comparative study [18], it has also been demonstrated that C3 and REV perform very well for a number of time series, among which the Hénon Map. However, it was also found that these measures can fail completely in other cases. Indeed, when in-band noise is added to the Mackey-Glass time series, the power of both C3 and REV drops dramatically, whereas the power of the proposed DVV method remains intact for noise levels of about $a = 0.8$. In the case of the Laser time series, the robustness of the DVV method is comparable to that of C3, but REV performs poorly in the presence of noise.

B. Biomedical Time Series

The minimal target variances for four of the HRV time series (A1–A4) are shown in Fig. 6(A). It is clear that the minimal target variance is higher for A2 than for the other HRV time

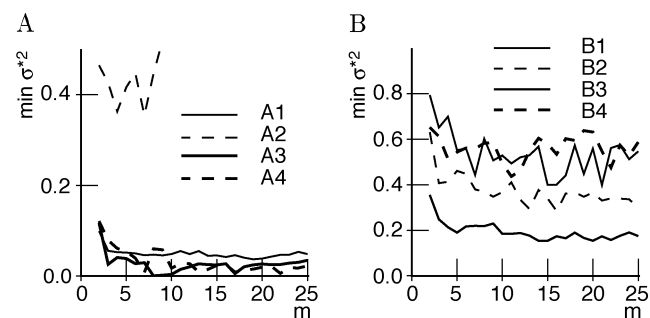


Fig. 6. Minimal target variance σ^{*2} as a function of embedding dimension m for the HRV time series (A) and for the fMRI time series (B).

series (also higher than for A5 and A6, results of which are not shown), which is an indication of a more stochastic nature. The optimal embedding dimensions and the time lags for C3 and REV, determined using the TDMI, are included in Table I.

The results from the nonlinearity detection analyses show that the surrogate-based methods (C3, REV, and DVV) find indications of nonlinearity in most of the time series. The prediction gain is small ($\gamma < 0.03$) for A1, A2, and A5, indicating that these time series are linear. Using C3 and REV, time series A4 and A5, and, respectively, A2 are judged linear. The RMSE values from the DVV methods show that A2 yields the smallest deviation from the linearity hypothesis. The DVV scatter diagrams are shown in Fig. 7 for A1–A4. Again, it is clear that A2 exhibits more linear behavior: there is only a small deviation from the bisector line (RMSE = $9.11 \cdot 10^{-4}$).

The optimal embedding dimensions for the four fMRI time series are obtained from Fig. 6(B), and are included in Table I. The large minimal target variances are, at least in part, due to the small signal-to-noise ratio (SNR) of fMRI signals.

Table I shows the results from the nonlinearity detection analyses (and the time lags obtained using the TDMI). The prediction gain yields only a small indication of nonlinearity for B1, and is close to zero for the other fMRI signals. Furthermore, contrary to what is expected from the recording set-up, C3 rejects the null hypothesis of linearity for the MION signals (B3 and B4), and not for the BOLD ones (B1 and B2), and REV finds evidence for nonlinearity in B2 and B4. The proposed DVV method detects nonlinearity in B1, B2, and B4,

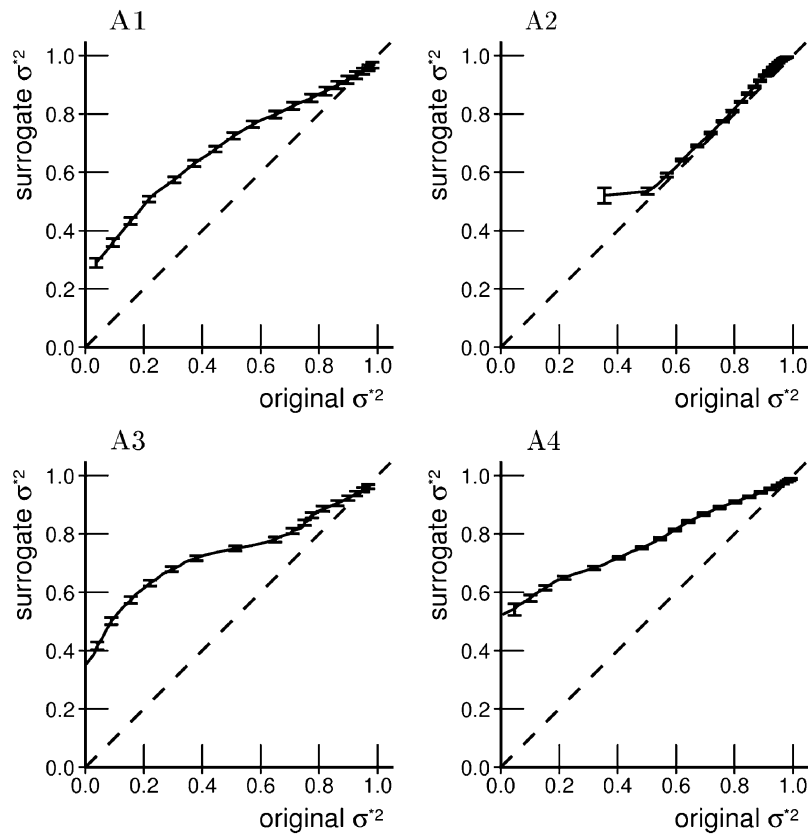


Fig. 7. DVV scatter diagrams for the HRV time series (A1–A4). The error bars correspond to the upper and lower quartiles of the target variances for the surrogates.

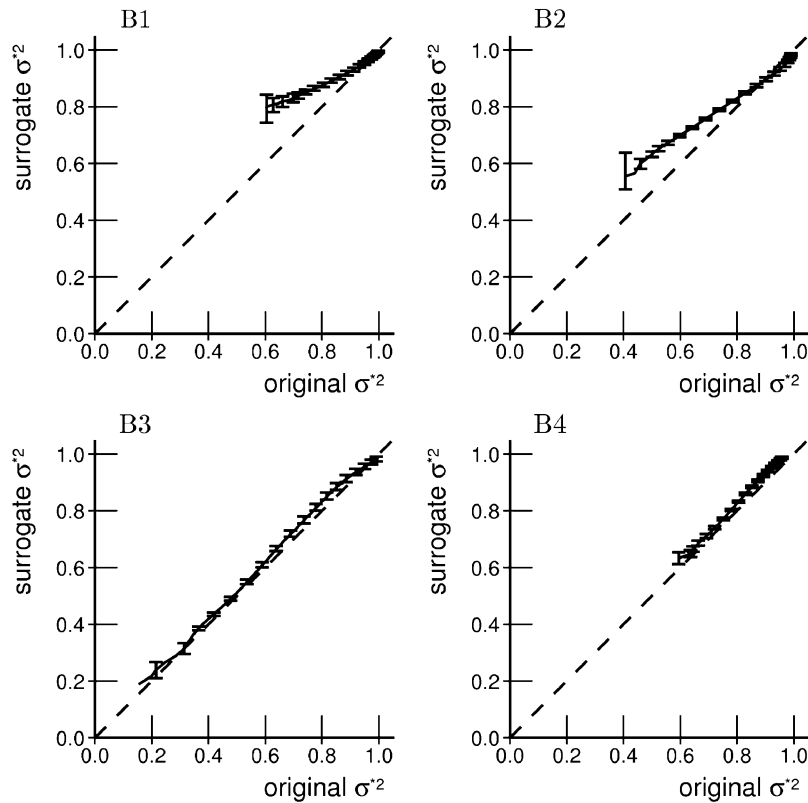


Fig. 8. DVV scatter diagrams for the fMRI time series (B1–B4). The error bars correspond to the upper and lower quartiles of the target variances for the surrogates.

and, additionally, the method reveals that the deviations from the bisector line (RMSE) are smaller for the MION signals (B3

and B4) than for the BOLD ones (B1 and B2), which complies with the recording conditions. This can also be observed in the

DVV scatter diagrams shown in Fig. 8: the diagrams for B3 and B4 almost coincide with the bisector line, whereas those for B1 and B2 do not.

V. CONCLUSION

We have introduced a novel methodology for characterizing the nature of a time series on the basis of its fundamental property, namely its predictability. The DVV method yields a standardized representation of the time series under study, allowing for a clear interpretation of its deterministic and/or stochastic nature in terms of its predictability. To gain further insight into the linear or nonlinear nature of the time series, the proposed DVV method has been combined with the surrogate data method [16]. Realizations of the null hypothesis that the original time series is linear are generated using the iAAFT method [12]. DVV-plots are computed for both the original and the surrogate time series, and, owing to the standardization within the method, the results can be conveniently visualized in a “DVV scatter diagram.” Indications of nonlinearity can then be observed as deviations from the bisector line, and can be quantified as the RMSE between the DVV-plots for the original and the surrogate time series. A nonparametric rank-based approach is used for testing the validity of the null hypothesis of linearity [16]. Furthermore, apart from a statistical test, the RMSE allows for a quantitative comparison of the indications of nonlinearity between signals. Note that in this setting, nonlinearity is defined as a deviation from the null hypothesis that the time series under study is generated by a linear stochastic model driven by white Gaussian noise, possibly followed by a static nonlinear observation function, and that a rejection of this null hypothesis does not yield information regarding what aspect of the null hypothesis is violated.

The proposed method was first verified on four benchmark time series, three of which were synthetically generated, whereas the fourth one was a real-world example of a known nature. The results were compared to three other methods, namely the prediction gain when nonlinearities are incorporated within the prediction model [1], the third-order autocovariance (C3) and the asymmetry due to time reversal (REV), the latter two of which also adopt the surrogate data strategy [18]. The performance of the DVV method was comparable to that of the two surrogate-based methods, and correctly detected nonlinearities in three of the four benchmark time series, as did the prediction gain. One should note, however, that the choice of the time lag, τ , for the C3 and REV methods were chosen to optimize a correct detection of the linear or nonlinear nature of the time series under study. The embedding dimensions used in the DVV analyses were not optimized for a correct detection, but for an optimal standardized representation of the time series. Furthermore, the quantitative measures of nonlinearity were different between the DVV-method (the RMSE) and the prediction gain. This could be due to the limited implementation of the nonlinear prediction model, namely a second-order Volterra model. In a next step, the robustness of the surrogate-based methods with respect to additive, in-band noise was examined. It was found that the DVV method was

more robust to noise, albeit the performance varied with the time series used for the analysis. Overall, the proposed DVV method seems to correctly detect the presence of nonlinearity in a wider variety of signals than C3 and REV.

The methods were then applied to two types of biomedical time series. The first set consisted of heart rate variability (HRV) time series obtained for patients suffering from different heart diseases. It has been suggested on several occasions that the presence of nonlinearities in HRV signals convey information regarding the health status of a patient [1]–[4], and, thus, that different heart diseases have a different effect on the nature of HRV signals. All surrogate-based methods found evidence for nonlinearities in most HRV time series, whereas the prediction gain only found indications of nonlinearity in three out of six, again, possibly due to the limitation of the second-order Volterra model. Additionally, the proposed DVV method indicated that time series A2, for which no significant rejection of linearity hypothesis was found using REV, deviated the least from the hypothesis of linearity, and was more stochastic in nature than the other HRV time series.

Finally, the difference in nonlinearity is examined between two types of time series recorded using functional Magnetic Resonance Imaging (fMRI). For the first set, the traditional blood oxygen level dependent (BOLD) technique was used, whereas for the second set, an exogenous contrast agent, Monocrystalline Iron Oxide Nanoparticle (MION) was employed. The BOLD signals are dependent on cerebral blood flow, volume and metabolic rate of oxygen, which interact possibly in a nonlinear fashion, whereas the MION signals are only governed by cerebral blood volume [11], [22]. Therefore, assuming that these physiological variables are (possibly nonlinearly) coupled, the time series recorded using the BOLD technique should show more indications of nonlinearity than those recorded using MION. The results from the prediction gain, C3 and REV did not support this hypothesis. The proposed DVV method, however, detected nonlinearity in three out of four time series (two BOLD and one MION), and showed a stronger deviation from linearity for the BOLD signals. Furthermore, the DVV-plots detected a fairly strong stochastic component in all time series, which is, at least partially, attributable to the typically low SNR of fMRI signals.

The proposed DVV method has been shown to perform well on benchmark signals, and even to outperform some of the well-established techniques for the detection of signal nonlinearity. The results on two types of biomedical time series are in line with current hypotheses regarding the nonlinearities present, clearly showing the usefulness of the proposed method. Due to the standardization within the algorithm, and the straightforwardly interpretable results, it can be readily applied to other biomedical time series where the presence of nonlinearities can be used as an indication of the health status of a patient.

ACKNOWLEDGMENT

The authors would like to thank W. Vanduffel and G.A. Orban, K.U. Leuven, for providing the fMRI data, and the anonymous reviewers for their critical comments.

REFERENCES

- [1] D. J. Christini, F. M. Bennett, K. R. Lutchin, H. M. Ahmed, J. M. Hausdorff, and N. Oriol, "Applications of linear and nonlinear time series modeling to heart rate dynamics analysis," *IEEE Trans. Biomed. Eng.*, vol. 42, pp. 411–415, Apr. 1995.
- [2] S. Guzzetti, M. G. Signorini, C. Cogliati, S. Mezzetti, A. Porta, S. Cerutti, and A. Malliani, "Non-linear dynamics and chaotic indices in heart rate variability of normal subjects and heart-transplanted patients," *Cardiovasc. Res.*, vol. 31, pp. 441–446, 1996.
- [3] K. K. Ho, G. B. Moody, C. K. Peng, J. E. Mietus, M. G. Larson, D. Levy, and A. L. Goldberger, "Predicting survival in heart failure case and control subjects by use of fully automated methods for deriving nonlinear and conventional indices of heart rate dynamics," *Circulation*, vol. 96, pp. 842–848, 1997.
- [4] C.-S. Poon and C. K. Merrill, "Decrease of cardiac chaos in congestive heart failure," *Nature*, vol. 389, pp. 492–495, 1997.
- [5] D. P. Mandic and J. A. Chambers, *Recurrent Neural Networks for Prediction: Learning Algorithms Architecture and Stability*. Chichester, U.K.: Wiley, 2001.
- [6] M. C. Casdagli and A. S. Weigend, "Exploring the continuum between deterministic and stochastic modeling," in *Time Series Prediction: Forecasting the Future and Understanding the Past*, A. S. Weigend and N. A. Gershenfeld, Eds. Reading, MA: Addison-Wesley, 1994.
- [7] T. Schreiber and A. Schmitz, "Surrogate time series," *Physica D*, vol. 142, no. 3–4, pp. 346–382, 2000.
- [8] H. O. A. Wold, *A Study in the Analysis of Stationary Time Series*. Uppsala, Sweden: Almqvist and Wiksell, 1938.
- [9] A. S. Weigend and N. A. Gershenfeld, Eds., *Time Series Prediction: Forecasting the Future and Understanding the Past*. Reading, MA: Addison-Wesley, 1994.
- [10] W. Vanduffel, D. Fize, J. B. Mandeville, K. Nelissen, P. Van Hecke, B. R. Rosen, R. B. H. Tootell, and G. A. Orban, "Visual motion processing investigated using contrast-agent enhanced fMRI in awake behaving monkeys," *Neuron*, vol. 32, no. 4, pp. 565–577, 2001.
- [11] K. J. Friston, A. Mechelli, R. Turner, and C. J. Price, "Nonlinear responses in fMRI: the balloon model, Volterra kernels, and other hemodynamics," *NeuroImage*, vol. 12, pp. 466–477, 2000.
- [12] T. Schreiber and A. Schmitz, "Improved surrogate data for nonlinearity tests," *Phys. Rev. Lett.*, vol. 77, pp. 635–638, 1996.
- [13] D. Kugiumtzis, "Test your surrogate data before you test for nonlinearity," *Phys. Rev. E*, vol. 60, pp. 2808–2816, 1999.
- [14] D. T. Kaplan, "A model-independent technique for determining the embedding dimension," in *Chaos in Communications*, L. M. Pecora, Ed. Bellingham, WA: SPIE, 1993, vol. 2038, pp. 236–240.
- [15] J. Theiler, P. S. Linsay, and D. M. Rubin, "Detecting nonlinearity in data with long coherence times," in *Time Series Prediction: Forecasting the Future and Understanding the Past*, A. S. Weigend and N. A. Gershenfeld, Eds. Reading, MA: Addison-Wesley, 1994, pp. 429–455.
- [16] J. Theiler and D. Prichard, "Constrained-realization Monte-Carlo method for hypothesis testing," *Physica D*, vol. 94, pp. 221–235, 1996.
- [17] H. Akaike, "A new look at the statistical model identification," *IEEE Trans. Automat. Contr.*, vol. AC-9, pp. 716–723, 1974.
- [18] T. Schreiber and A. Schmitz, "On the discrimination power of measures for nonlinearity in a time series," *Phys. Rev. E*, vol. 55, pp. 5443–5447, 1997.
- [19] C. Diks, J. C. van Houwelingen, F. Takens, and J. DeGoede, "Reversibility as a criterion for discriminating time series," *Phys. Lett. A*, vol. 201, pp. 221–228, 1995.
- [20] A. M. Fraser and H. L. Swinney, "Independent coordinates for strange attractors from mutual information," *Phys. Rev. A*, vol. 33, no. 2, pp. 1134–1140, 1986.
- [21] R. Hegger, H. Kantz, and T. Schreiber, "Practical implementation of nonlinear time series methods: the TISEAN package," *Chaos*, vol. 9, pp. 413–435, 1999.
- [22] J. B. Mandeville, J. J. Marota, C. Ayata, G. Zarachuk, M. A. Moskowitz, B. Rosen, and R. M. Weisskoff, "Evidence of a cerebrovascular postarteriole windkessel with delayed compliance," *J. Cereb. Blood Flow Metab.*, vol. 19, pp. 679–689, 1999.



Temujin Gautama received the B.Sc. degree in electrical engineering from Groep T, Leuven, Belgium, the M.Sc. degree in artificial intelligence from the K.U.Leuven, Leuven, Belgium, and the Ph.D. degree in medical sciences from the K.U.Leuven.

He is currently with the Laboratorium voor Neuro- en Psychofysiologie at the Medical School of the K.U.Leuven. His research interests include nonlinear signal processing, biological modeling, and self-organizing neural networks and their application to data mining.



Danilo P. Mandic (M'99) received the B.Sc. (Hons.) degree in electrical and electronic engineering, and the M.Sc. degree in signal processing, from the University of Banja Luka, Bosnia-Herzegovina. He received the Ph.D. degree in nonlinear adaptive signal processing from the Imperial College, London, U.K.

He is currently Senior Lecturer in Signal Processing in the Department of Electrical and Electronic Engineering of the Imperial College of Science, Technology and Medicine, London, U.K. His areas of interest include linear and nonlinear

adaptive signal processing, system identification, stability theory, and computer vision.

Dr. Mandic has received awards for his collaboration with industry, and was also awarded the Nikola Tesla Medal for his innovative work.



Marc M. Van Hulle received the M.Sc. degree in electrotechnical engineering (electronics) and the Ph.D. degree in applied sciences from the K.U.Leuven, Leuven, Belgium, in 1985 and 1990, respectively. He also holds the B.Sc.Econ. and MBA degrees.

Since 1992, he has been a Postdoctoral Scientist with the Brain and Cognitive Sciences Department at the Massachusetts Institute of Technology (MIT), Boston. He is also affiliated with the Neuro- and Psychophysiology Laboratory, Medical School,

K.U.Leuven, as an Associate Professor. His research interests include neural networks, biological modeling, vision, data mining, and signal processing.

Dr. Van Hulle is an Executive Member of the IEEE Signal Processing Society, Neural Networks for Signal Processing (NNSP) Technical Committee (1996–1999, 2000–2003), the Publicity Chair of NNSP's 1999 and 2000 workshops, and the Program co-chair of NNSP's 2001, 2002 and 2003 workshops, and reviewer and co-editor of several special issues for several neural network and signal processing journals.